Supplemental Information: Evaluating Long-term Seasonal Variability of Aerosol Optical Properties in Colorado

Erin K. Boedicker[1,2], Andre Bergeron[3], Gerardo Carrillo-Cardenas[4], Dominik Kulakowski[3], John Rogan[3], Elisabeth Andrews[1,2], A. Gannet Hallar[4]

[1]NOAA Earth System Research Laboratory, Boulder, CO 80305, USA
[2]Cooperative Institute for Research in Environmental Sciences, University of Colorado, Boulder, CO 80309, USA
[3]Graduate School of Geography, Clark University, Worcester, MA 01016, USA
[4]Department of Atmospheric Sciences, University of Utah, Salt Lake City, UT 84112, USA

Correspondence to: Gannet Hallar (Gannet.Hallar@utah.edu)

Section S1: Measurement comparisons for SPL PSAP and CLAP data
Section S2: Description of auxiliary calculations
Section S3: Further information on climatology of aerosol optical properties
Section S4: Additional figures and information for trend analysis
Section S4: Further information on the seasonality and systematic variability of derived optical properties

Section S1: Measurement comparisons for SPL PSAP and CLAP data

At SPL, aerosol absorption coefficients (σ_{ap}) were measured using both a Particle Soot Absorption Photometer (PSAP; Radiance Research) and a Continuous Light Absorption Photometer (CLAP; NOAA; Ogren et al., 2017). The PSAP operated from 2011 – 2018, and the CLAP has been run from 2011 to the present. Both instruments measure absorption at three wavelengths – the PSAP at 467, 530, and 660 nm, and the CLAP at 467, 528, and 652 nm – and have previously been shown to be comparable measurements (Ogren et al., 2017). While data from this paper uses only the CLAP data from SPL, the previous analysis done by Japngie-Green et al. (2019) used data from the PSAP from 2011 – 2013 and CLAP data from 2013 – 2016. Since this paper follows work done by Japngie-Green et al. (2019) but only uses CLAP data, the PSAP and CLAP measurements were compared to ensure that the two sampling methods were in relative agreement. Data in this comparison includes all PSAP and CLAP measurements from 2012 – 2016, and wavelengths were adjusted to match the TSI scattering measurements (450, 550, and 700 nm). Measurements were corrected for scattering and filter artifacts, sample area, flowrate, and non-idealities in the manufacturer's calibration (Bond et al., 1999; Ogren, 2010).

Table S1: Summary of linear regression comparisons between PSAP and CLAP data

Absorption coefficient (σ_{ap}) comparison

	450 nm		550 nm		700 nm	
	Slope	Int.	Slope	Int.	Slope	Int.
Hourly	0.884 ± 0.002	0.093 ± 0.004	0.941 ± 0.001	0.012 ± 0.002	0.870 ± 0.001	0.039 ± 0.002
Daily	0.880 ± 0.004	0.090 ± 0.008	0.911 ± 0.005	0.053 ± 0.007	0.856 ± 0.005	0.066 ± 0.006

Absorption Ångström exponent (AAE) comparison

	450 & 550 nm		450 & 700 nm		550 & 700 nm	
	Slope	Int.	Slope	Int.	Slope	Int.
Hourly	0.786 ± 0.006	0.25 ± 0.01	0.852 ± 0.05	0.35 ± 0.01	0.822 ± 0.007	0.51 ± 0.01
Daily	0.80 ± 0.02	0.24 ± 0.03	0.85 ± 0.02	0.36 ± 0.03	0.84 ± 0.02	0.50 ± 0.03
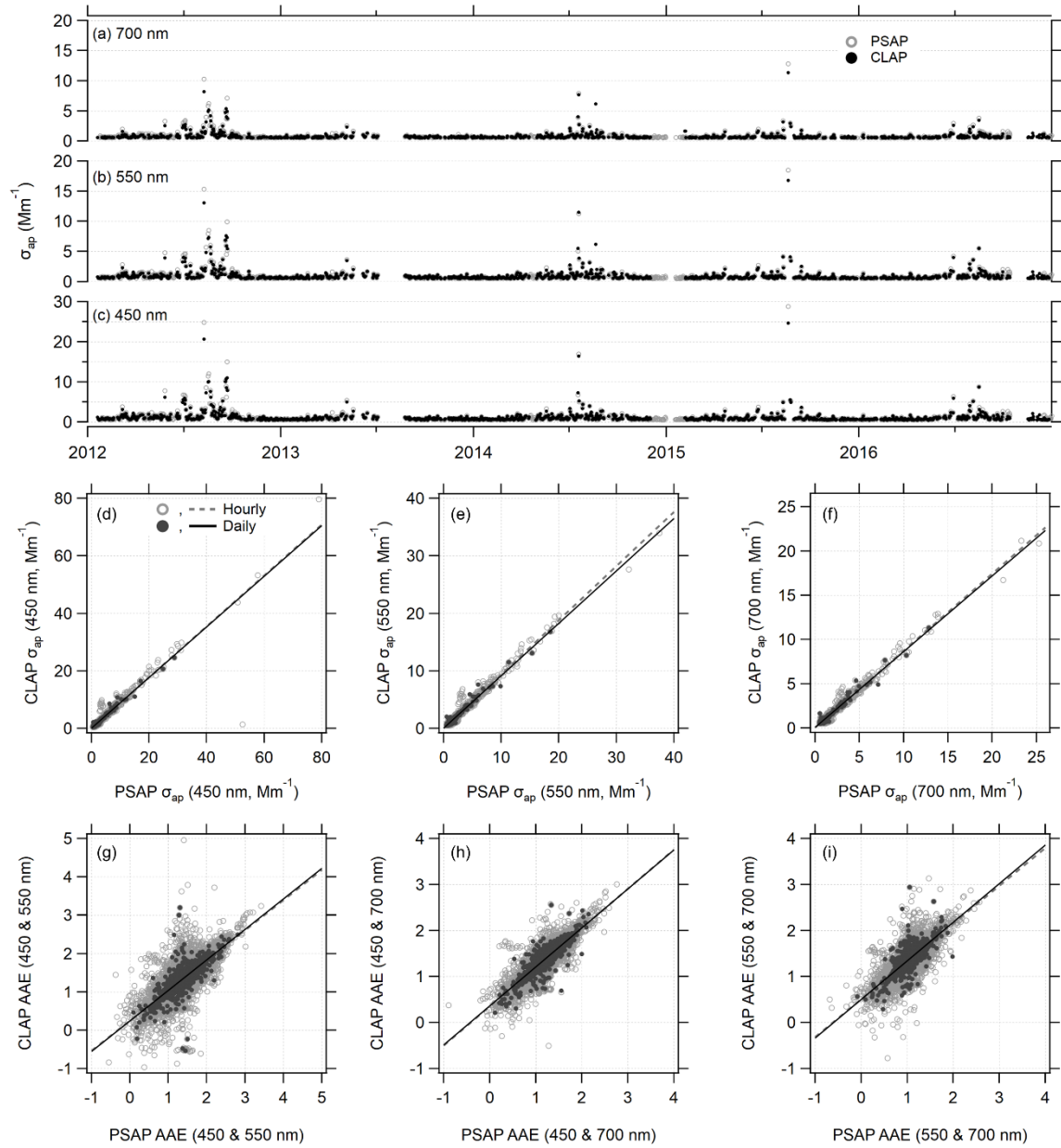
35 **Figure S1**: Intercomparison of CLAP and PSAP data. Timeseries show daily median σ_{ap} at all three wavelengths: (a) 450 nm, (b) 550 nm, and (c) 700 nm. The bottom plots show intercomparisons between hourly and daily averaged σ_{ap} data at (d) 450 nm, (e) 550 nm, and (f) 700 nm, and AAE values for (g) 450 & 550 nm, (h) 450 & 700 nm, and (i) 550 & 700 nm. In all intercomparison plots open markers show hourly averaged data, dashed lines show the linear relationship for hourly averaged data, closed markers show the daily averaged data, and solid lines show the linear relationship for the daily averaged data.

Section S2: Description of auxiliary data treatment and calculations

Wavelength adjustment of absorption coefficient

In order to harmonize the wavelengths of the scattering and absorption coefficient measurements, we adjusted the wavelengths of the absorption coefficients (467, 528, and 652 nm) to match those of the scattering coefficients (450, 550, 700 nm). This is often called the Angstrom adjustment:

$$\sigma_{ap,i} = \sigma_{ap,j} \left(\frac{\lambda_i}{\lambda_j}\right)^{AAE}, \tag{S1}$$

where AAE is the absorption Angstrom exponent defined in equation 4 of the main text, λ represents wavelength, and the i and j subscripts indicate the adjusted and measured wavelength, respectively.

Filtering for calculated parameters

Calculated parameters are more heavily influenced by instrument noise and are less reliable when σ_{sp} and σ_{ap} values are low. For this reason, filtering of the calculated parameters was done to exclude values where $\sigma_{sp} < 1$ Mm^{-1} and $\sigma_{ap} < 0.5$ Mm^{-1}. This filtering predominately affected parameters related to absorption, and the SPL data was more heavily impacted as the site has lower overall aerosol loadings. Approximately 9%, 14%, 52%, 65% of the BFR, SAE, SSA, and AAE data at SPL, and approximately 1%, 2%, 14%, and 21% of the BFR, SAE, SSA, and AAE data at BOS were removed due to these constraints. However, the overall statistical values for the variables were not significantly changed as a result (**Table S2**).

Table S2: Unfiltered and filtered optical data from SPL and BOS using the $\sigma_{sp} > 1$ Mm^{-1} and $\sigma_{ap} > 0.5$ Mm^{-1} bounds. Number of hourly data points is reported, along with the 25th, 50th, and 75th percentile values for each optical parameter.

		BFR		SAE		SSA		AAE	
		unfiltered	filtered	unfiltered	filtered	unfiltered	filtered	unfiltered	filtered
SPL	# hourly data points	105838	96502	105776	91431	86358	41359	89303	30912
	75th	0.181	0.177	2.024	1.999	0.941	0.938	1.65	1.667
	50th	0.158	0.157	1.736	1.735	0.924	0.925	1.402	1.446
	25th	0.137	0.139	1.339	1.369	0.900	0.907	1.073	1.24
BOS	# hourly data points	44781	44327	44729	43726	40549	34917	43562	34397
	75th	0.170	0.170	1.935	1.931	0.925	0.923	1.546	1.505
	50th	0.152	0.152	1.685	1.685	0.899	0.897	1.375	1.358
	25th	0.135	0.135	1.352	1.352	0.864	0.860	1.204	1.200

Calculation of an upper bound for σ$_{sp}$

60   To determine an appropriate upper limit for identifying spikes, a simple outlier calculation was done on the data for each month based on the interquartile range (IQR). The upper limit was based on the equation:

$$\sigma_{sp,upper} = Q75 + (IQR \times 1.5) \,, \tag{S2}$$

where Q75 represents the 75th percentile and IQR represents the interquartile range of the measurements. The average monthly σ$_{sp,upper}$ for the entire data range of the SPL and BOS σ$_{sp}$ data were 30 ± 40 Mm^{-1} and 50 ± 50 Mm^{-1} respectively. For both SPL

65   and BOS, the highest calculated upper bounds were in the summer months (**Table S3**). In the analysis presented, a uniform value of 50 Mm^{-1} was used in the identification of spikes to reasonably capture possible outlier events at both sites and to ensure consistent treatment of the data.

70   **Table S3**: Calculated σ$_{sp,upper}$ (Mm^{-1}) values by season for SPL and BOS.

	Winter (Dec -Feb)	Spring (March – May)	Summer (June – Aug)	Fall (Sep – Nov)
	$\mu \pm \sigma$ (min – max)	$\mu \pm \sigma$ (min – max)	$\mu \pm \sigma$ (min – max)	$\mu \pm \sigma$ (min – max)
SPL	7 ± 3 (3 – 19)	19 ± 6 (7 – 30)	50 ± 60 (15 – 297)	30 ± 30 (5 – 169)
BOS	40 ± 20 (19 – 107)	40 ± 10 (20 – 66)	80 ± 70 (25 – 302)	60 ± 50 (21 – 201)

Section S3: Further information on climatology of aerosol optical properties
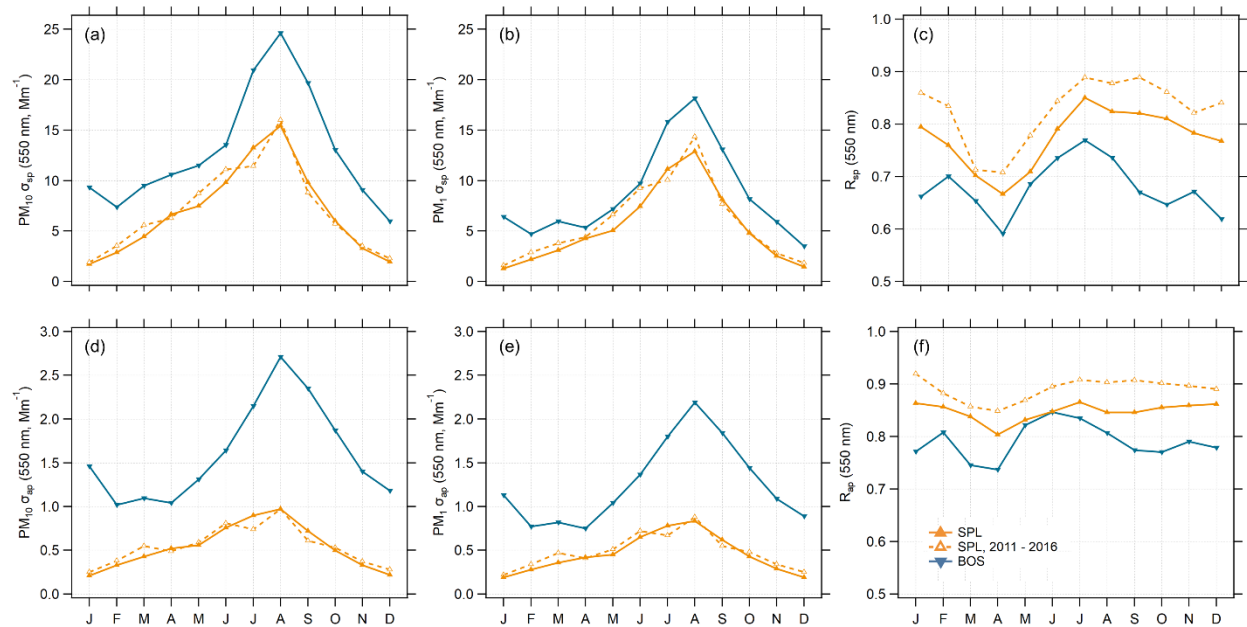
Figure S2: Monthly median (a) PM_{10} σ_{sp} at 550 nm, (b) PM_1 σ_{sp} at 550 nm, (c) sub-micron scattering (R_{sp}) fractions, (d) PM_{10} σ_{ap} at 550 nm, (e) PM_1 σ_{ap} at 550 nm, and (f) sub-micron absorption (R_{ap}) fractions. Medians for the entire SPL data range are shown as solid orange traces with closed markers, and medians for the 2011-2016 period are shown as dashed lines with open markers. Data for BOS is shown by the solid blue trace with closed markers.
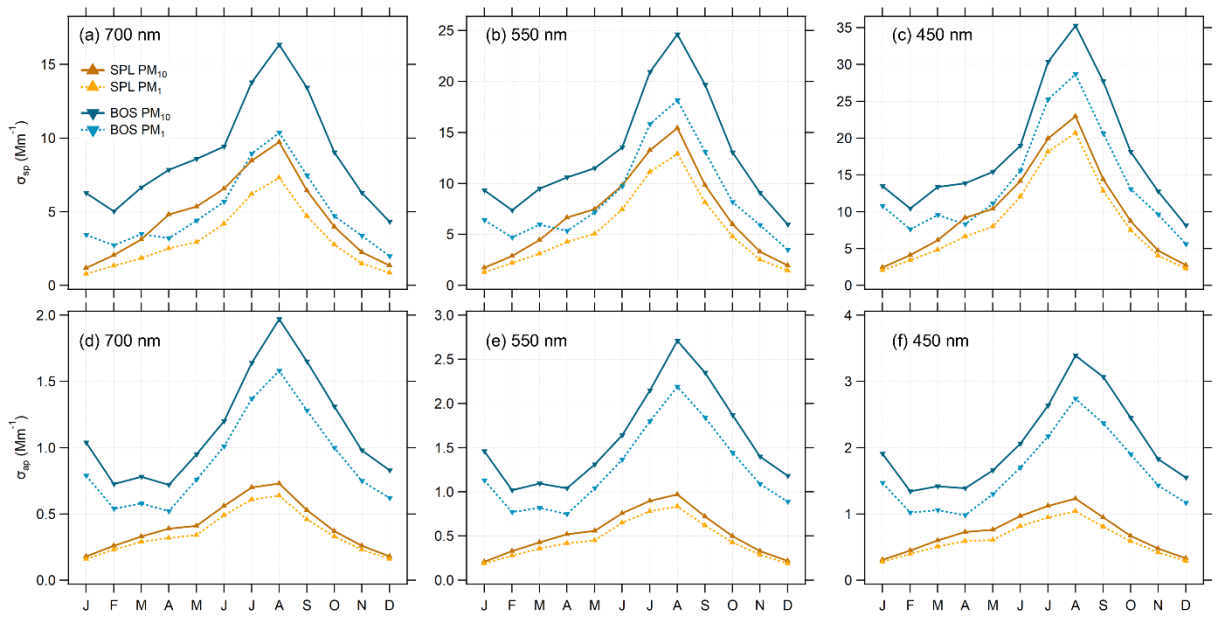
Figure S3: Monthly median values of σ_{sp} at (a) 700 nm, (b) 550 nm, and (c) 450 nm in the top row of figures, and σ_{ap} at (d) 700 nm, (e) 550 nm, and (f) 450 nm in the bottom row of figures. Data for SPL is shown in orange, and data for BOS is shown in blue. PM$_{10}$ data is represented with solid lines and PM$_1$ data is shown as dashed lines. Note the changes in y-axis between the figures.
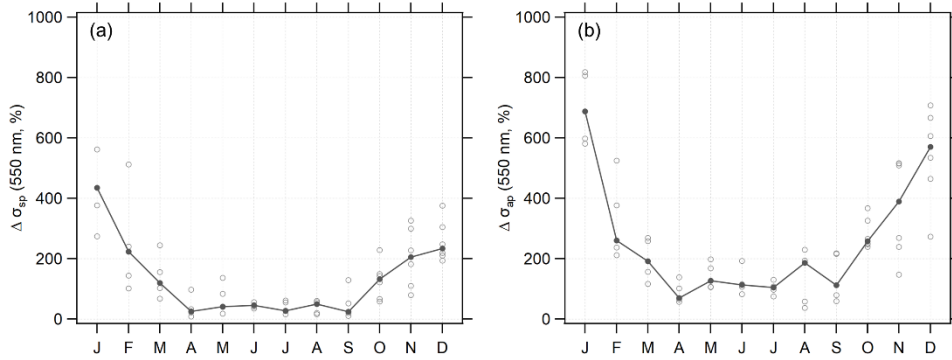
Figure S4: Percent difference between BOS and SPL (a) σ_{sp} and (b) σ_{ap} monthly median values for the 550 nm measurement. Values were calculated using: $\Delta\sigma = (\sigma_{BOS} - \sigma_{SPL}) / \sigma_{SPL} \times 100$. Open markers show the calculated value by month, and the solid grey trace shows the median percent difference.
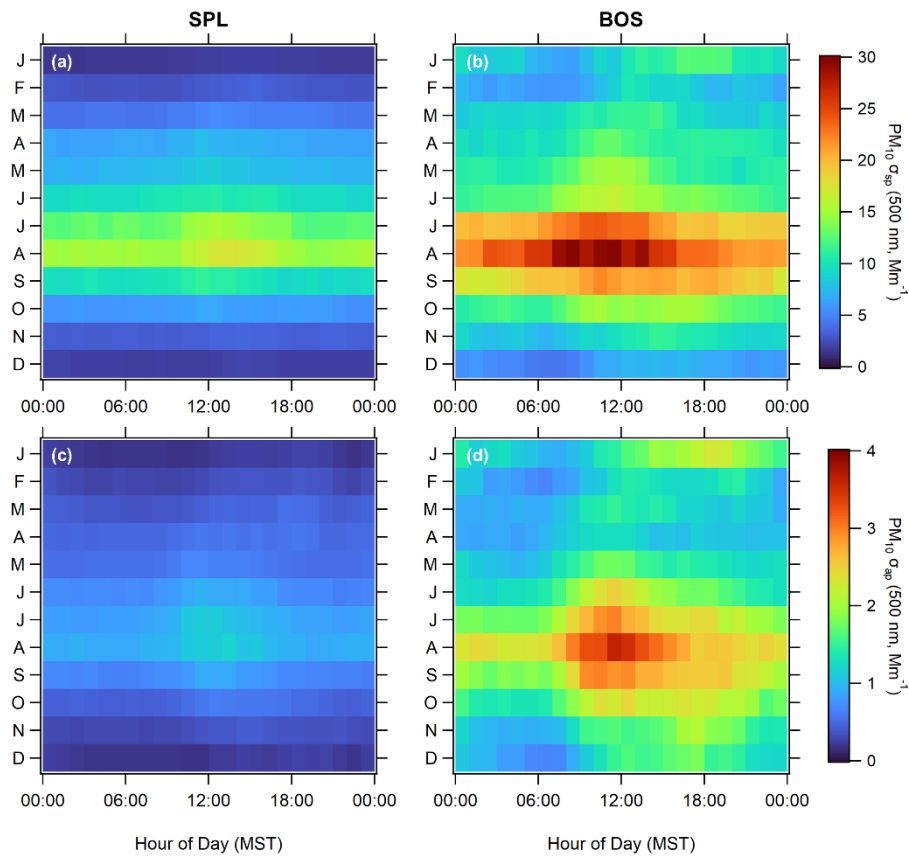
95 **Figure S5**: Monthly diurnal cycles of median scattering for (a) SPL and (b) BOS, and median absorption for (c) SPL and (d) BOS.
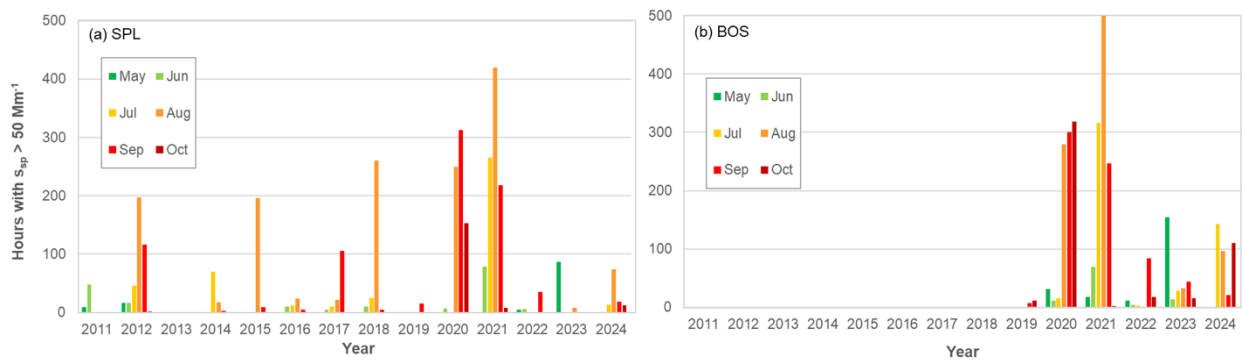
Figure S6: Number of hours at (a) SPL and (b) BOS during the months of May to October, where σ_{sp} was greater than 50
100 Mm^{-1}.

Table S4: Number of hours that exceed the 50 Mm^{-1} upper bound by year and month at SPL and BOS. Bold numbers show the total yearly and monthly number of hours and July – September data are shaded as they are the three months with the most instances of exceedance at both sites. If no data is available for a given month and year, then the table was left blank.

	2011	2012	2013	2014	2015	2016	2017	2018	2019	2020	2021	2022	2023	2024	
SPL															
Jan	0	0	0	0	0	0	0	0	0	0	0	0	0	0	**0**
Feb	0	0	0	0	0	0	0	0	0	0	0	0	0	0	**0**
Mar	18	4	0	0	0	0	0	5	0	0	1	0	1	0	**29**
Apr	12	1	0	0	4	0	2	0	0	1	0	3	3	0	**26**
May	9	17	0	0	0	0	0	0	0	0	1	5	87	0	**119**
Jun	48	16	0	1	0	10	5	10	0	7	78	6	0	1	**182**
Jul	0	46	0	70	0	12	10	25	0	1	265	0	1	13	**443**
Aug	0	197	0	18	196	24	22	260	0	250	420	1	8	74	**1470**
Sep	0	116	0	3	9	5	106	5	15	313	218	35	1	19	**845**
Oct	0	2	0	0	0	0	0	0	1	153	8	0	0	12	**176**
Nov	0	0	0	0	0	0	0	0	0	0	0	0	0	0	**0**
Dec	0	0	0	0	0	0	1	0	0	0	0	0	0	0	**1**
	87	**399**	**0**	**92**	**209**	**51**	**146**	**305**	**16**	**725**	**991**	**50**	**101**	**119**	
BOS															
Jan										14	57	26	102	17	**216**
Feb										32	149	20	6	1	**208**
Mar										55	98	26	68	12	**259**
Apr										13	21	0	2	14	**50**
May										31	18	11	154	0	**214**
Jun										11	69	4	13	1	**98**
Jul										15	316	3	28	143	**505**
Aug										280	501	1	32	96	**910**
Sep									7	301	247	84	44	21	**704**
Oct									11	318	2	18	15	110	**474**
Nov									101	1	31	2	4	6	**145**
Dec									42	30	1	14	47	0	**134**
									161	**1101**	**1510**	**209**	**515**	**421**	

Section S4: Additional figures and information for trend analysis
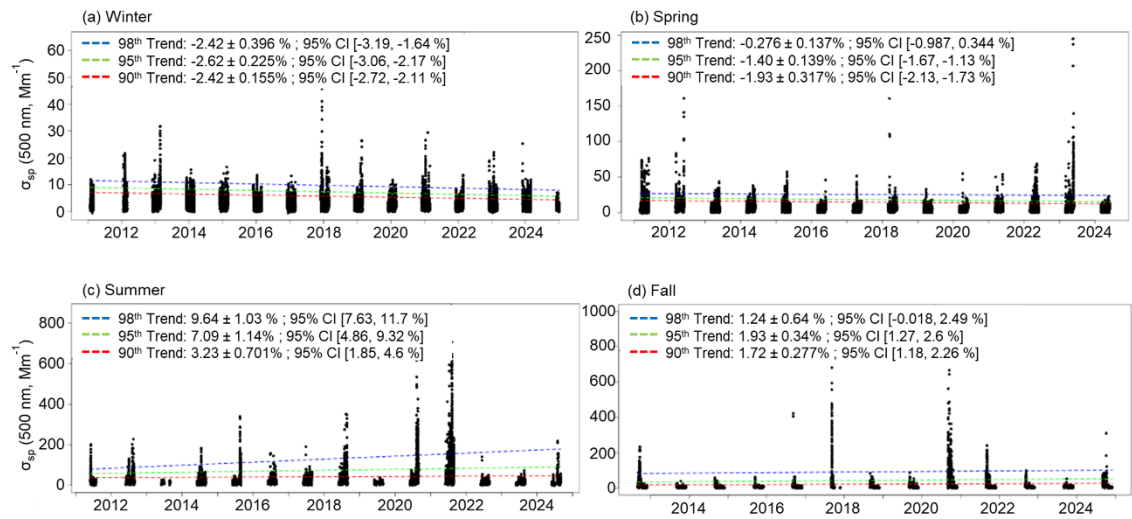
Figure S7: Seasonal quantile regression of σ_{sp} (550 nm) showing the trend (% yr^{-1}) for the 90th, 95th, and 98th percentile data in each season: (a) Winter, (b) Spring, (c) Summer, and (d) Fall.
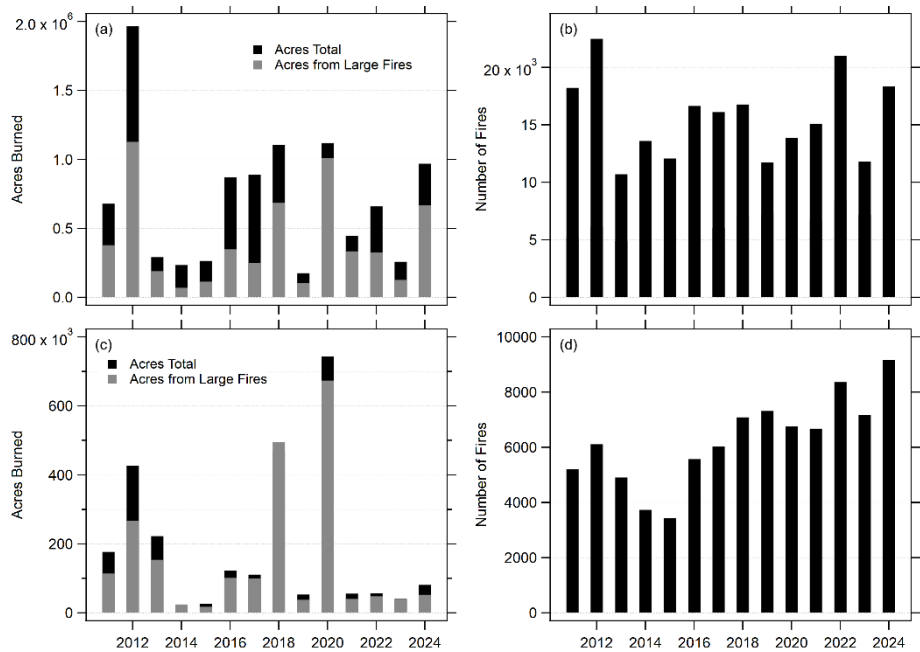
Figure S8: (left) Acres burned and (right) number of wildfires in Colorado by year. For the acres burned, the black bar shows the total acreage and the grey bar shows the acres burned by 'large fires' classified as fires that are 100 acres or more in timber fuel types, 300 acres or more in grass fuel types, or a fire that has a Type 1 or Type 2 IMT assigned. This data was extracted from the Rocky Mountain Area Coordination Center (RMACC) annual activity reports (https://gacc.nifc.gov/rmcc/intelligence.php).

Table S5: Results of the quantile regression analysis for σ_{sp} (550 nm). Trends are reported for each quantile in both Mm-1 yr-1 and % yr-1. The p-value is reported, and trend values that are insignificant are in grey text.

Quantile	Variable / Units	Winter	Spring	Summer	Fall
0.1	Trend: Mm^{-1} yr^{-1}	-0.016 ± 0.001	-0.024 ± 0.006	-0.04 ± 0.01	-0.001 ± 0.005
	Trend: % yr^{-1}	-1.1 ± 0.1	-1.0 ± 0.0.3	-0.7 ± 0.2	-0.1 ± 0.2
	p-value	<<0.001	<<0.001	<<0.001	0.789
0.2	Trend: Mm^{-1} yr^{-1}	-0.029 ± 0.002	-0.044 ± 0.006	-0.04 ± 0.01	0.019 ± 0.006
	Trend: % yr^{-1}	-1.7 ± 0.1	-1.3 ± 0.2	-0.5 ± 0.1	0.6 ± 0.2
	p-value	<<0.001	<<0.001	0.001	0.002
0.3	Trend: Mm^{-1} yr^{-1}	-0.038 ± 0.002	-0.094 ± 0.007	-0.03 ± 0.01	0.028 ± 0.008
	Trend: % yr^{-1}	-1.8 ± 0.1	-1.9 ± 0.1	-0.4 ± 0.1	0.7 ± 0.2
	p-value	<<0.001	<<0.001	0.005	<<0.001
0.4	Trend: Mm^{-1} yr^{-1}	-0.043 ± 0.003	-0.112 ± 0.008	-0.02 ± 0.01	0.06 ± 0.01
	Trend: % yr^{-1}	-1.7 ± 0.1	-1.8 ± 0.1	-0.2 ± 0.1	1.0 ± 0.2
	p-value	<<0.001	<<0.001	0.068	<<0.001
0.5	Trend: Mm^{-1} yr^{-1}	-0.056 ± 0.004	-0.129 ± 0.009	-0.03 ± 0.02	0.07 ± 0.01
	Trend: % yr^{-1}	-1.7 ± 0.1	-1.7 ± 0.1	-0.3 ± 0.1	0.8 ± 0.1
	p-value	<<0.001	<<0.001	0.062	<<0.001
0.6	Trend: Mm^{-1} yr^{-1}	-0.075 ± 0.005	-0.14 ± 0.01	-0.08 ± 0.02	0.09 ± 0.01
	Trend: % yr^{-1}	-1.9 ± 0.1	-1.6 ± 0.1	-0.6 ± 0.2	0.7 ± 0.1
	p-value	<<0.001	<<0.001	<<0.001	<<0.001
0.7	Trend: Mm^{-1} yr^{-1}	-0.096 ± 0.006	-0.19 ± 0.01	-0.12 ± 0.03	0.15 ± 0.02
	Trend: % yr^{-1}	-2.0 ± 0.1	-1.8 ± 0.1	-0.8 ± 0.2	0.9 ± 0.1
	p-value	<<0.001	<<0.001	<<0.001	<<0.001
0.8	Trend: Mm^{-1} yr^{-1}	-0.123 ± 0.007	-0.28 ± 0.02	-0.02 ± 0.07	0.24 ± 0.03
	Trend: % yr^{-1}	-2.0 ± 0.1	-2.0 ± 0.1	-0.1 ± 0.4	1.0 ± 0.1
	p-value	<<0.001	<<0.001	0.824	<<0.001
0.90	Trend: Mm^{-1} yr^{-1}	-0.19 ± 0.01	-0.40 ± 0.02	0.7 ± 0.2	0.7 ± 0.1
	Trend: % yr^{-1}	-2.4 ± 0.2	-1.9 ± 0.1	3.2 ± 0.7	1.7 ± 0.3
	p-value	<<0.001	<<0.001	<<0.001	<<0.001
0.92	Trend: Mm^{-1} yr^{-1}	-0.20 ± 0.01	-0.44 ± 0.03	0.9 ± 0.2	0.8 ± 0.2
	Trend: % yr^{-1}	-2.5 ± 0.2	-1.9 ± 0.1	3.5 ± 0.9	1.2 ± 0.2
	p-value	<<0.001	<<0.001	<<0.001	<<0.001
0.94	Trend: Mm^{-1} yr^{-1}	-0.22 ± 0.02	-0.44 ± 0.03	2.0 ± 0.3	1.2 ± 0.2
	Trend: % yr^{-1}	-2.5 ± 0.2	-1.6 ± 0.1	6 ± 1	1.8 ± 0.4
	p-value	<<0.001	<<0.001	<<0.001	<<0.001
0.96	Trend: Mm^{-1} yr^{-1}	-0.24 ± 0.02	-0.36 ± 0.06	3.3 ± 0.5	2.4 ± 0.4
	Trend: % yr^{-1}	-2.7 ± 0.2	-1.0 ± 0.2	9 ± 1	2.4 ± 0.4
	p-value	<<0.001	<<0.001	<<0.001	<<0.001
0.98	Trend: Mm^{-1} yr^{-1}	-0.23 ± 0.04	-0.1 ± 0.2	7.5 ± 0.8	1.6 ± 0.8
	Trend: % yr^{-1}	-2.4 ± 0.4	-0.3 ± 0.3	10 ± 1	1.2 ± 0.6
	p-value	<<0.001	0.383	<<0.001	0.053

Table S6: Results of the quantile regression analysis for SAE (450 & 700 nm). Trends are reported for each quantile in both Mm^{-1} yr^{-1} and % yr^{-1}. The p-value is reported, and trend values that are insignificant are in grey text.

Quantile	Variable / Units	Winter	Spring	Summer	Fall
0.1	Trend: Mm^{-1} yr^{-1}	-0.036 ± 0.002	-0.007 ± 0.001	0.002 ± 0.001	-0.017 ± 0.001
	Trend: % yr^{-1}	-3.5± 0.2	-1.0 ± 0.2	0.1 ± 0.1	-1.00 ± 0.09
	p-value	<<0.001	<<0.001	0.207	<<0.001
0.2	Trend: Mm^{-1} yr^{-1}	-0.026 ± 0.002	-0.007 ± 0.001	-0.003 ± 0.001	-0.015 ± 0.001
	Trend: % yr^{-1}	-2.1 ± 0.1	-0.7 ± 0.1	-0.21 ± 0.05	-0.83 ± 0.07
	p-value	<<0.001	<<0.001	<<0.001	<<0.001
0.3	Trend: Mm^{-1} yr^{-1}	-0.020 ± 0.001	-0.005 ± 0.001	-0.004 ± 0.001	-0.013 ± 0.001
	Trend: % yr^{-1}	-1.4 ± 0.1	-0.46 ± 0.09	-0.24 ± 0.05	-0.67 ± 0.05
	p-value	<<0.001	<<0.001	<<0.001	<<0.001
0.4	Trend: Mm^{-1} yr^{-1}	-0.017 ± 0.001	-0.006 ± 0.001	-0.005 ± 0.001	-0.011 ± 0.001
	Trend: % yr^{-1}	-1.05 ± 0.08	-0.47 ± 0.09	-0.29 ± 0.03	-0.54 ± 0.04
	p-value	<<0.001	<<0.001	<<0.001	<<0.001
0.5	Trend: Mm^{-1} yr^{-1}	-0.013 ± 0.001	-0.006 ± 0.001	-0.007 ± 0.001	-0.010 ± 0.001
	Trend: % yr^{-1}	-0.77 ± 0.08	-0.44 ± 0.08	-0.37 ± 0.03	-0.51 ± 0.04
	p-value	<<0.001	<<0.001	<<0.001	<<0.001
0.6	Trend: Mm^{-1} yr^{-1}	-0.012 ± 0.001	-0.006 ± 0.001	-0.007 ± 0.001	-0.011 ± 0.001
	Trend: % yr^{-1}	-0.63 ± 0.07	-0.37 ± 0.07	-0.36 ± 0.02	-0.51 ± 0.04
	p-value	<<0.001	<<0.001	<<0.001	<<0.001
0.7	Trend: Mm^{-1} yr^{-1}	-0.009 ± 0.001	-0.003 ± 0.001	-0.006 ± 0.001	-0.009 ± 0.001
	Trend: % yr^{-1}	-0.47 ± 0.06	-0.18 ± 0.06	-0.31 ± 0.02	-0.41 ± 0.03
	p-value	<<0.001	0.004	<<0.001	<<0.001
0.8	Trend: Mm^{-1} yr^{-1}	-0.006 ± 0.001	-0.002 ± 0.001	-0.006 ± 0.001	-0.009 ± 0.001
	Trend: % yr^{-1}	-0.28 ± 0.06	-0.11 ± 0.06	-0.28 ± 0.03	-0.40 ± 0.04
	p-value	<<0.001	0.089	<<0.001	<<0.001
0.90	Trend: Mm^{-1} yr^{-1}	-0.001 ± 0.001	-0.002 ± 0.001	-0.004 ± 0.001	-0.004 ± 0.001
	Trend: % yr^{-1}	-0.01 ± 0.07	-0.09 ± 0.07	-0.16 ± 0.03	-0.18 ± 0.05
	p-value	0.935	0.187	<<0.001	0.001
0.92	Trend: Mm^{-1} yr^{-1}	0.002 ± 0.002	-0.002 ± 0.002	-0.002 ± 0.001	-0.002 ± 0.001
	Trend: % yr^{-1}	0.07 ± 0.08	-0.10 ± 0.07	-0.11 ± 0.04	-0.09 ± 0.06
	p-value	0.421	0.160	0.005	0.108
0.94	Trend: Mm^{-1} yr^{-1}	0.003 ± 0.002	0.001 ± 0.002	-0.001 ± 0.001	0.001 ± 0.002
	Trend: % yr^{-1}	0.11 ± 0.08	0.1 ± 0.1	-0.01 ± 0.05	0.03 ± 0.07
	p-value	0.155	1.00	0.784	0.618
0.96	Trend: Mm^{-1} yr^{-1}	0.003 ± 0.003	0.001 ± 0.002	0.007 ± 0.002	0.002 ± 0.002
	Trend: % yr^{-1}	0.11 ± 0.08	0.04 ± 0.08	0.31 ± 0.08	0.14 ± 0.09
	p-value	0.371	0.595	<<0.001	0.109
0.98	Trend: Mm^{-1} yr^{-1}	0.001 ± 0.004	0.002 ± 0.003	0.034 ± 0.005	0.005 ± 0.004
	Trend: % yr^{-1}	0.1 ± 0.2	0.1 ± 0.1	1.4 ± 0.2	0.2 ± 0.1
	p-value	0.755	0.313	<<0.001	0.138

130

Section S5: Further information on the seasonality and systematic variability of derived optical properties
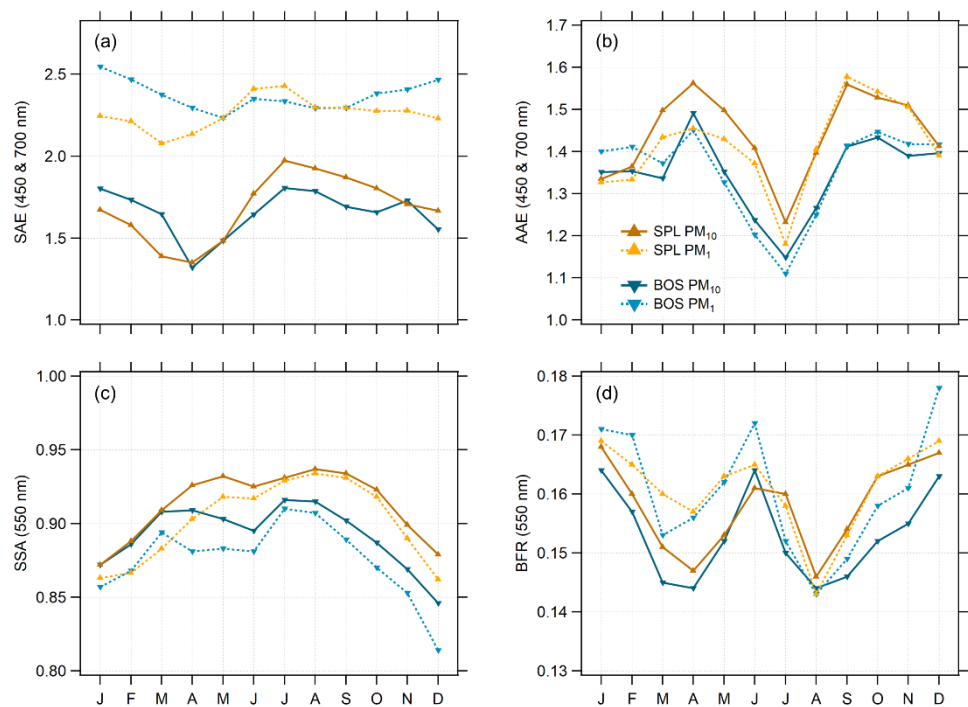
Figure S9: Monthly median values of (a) SAE for 450 & 700nm, (b) AAE for 450 & 700 nm, (c) SSA for 550 nm, and (d) BFR for 550 nm. Data for SPL is shown in orange and data for BOS is shown in blue. PM_{10} data is represented with solid lines and PM_1 data is shown as dashed lines. Note the changes in y-axis between the figures
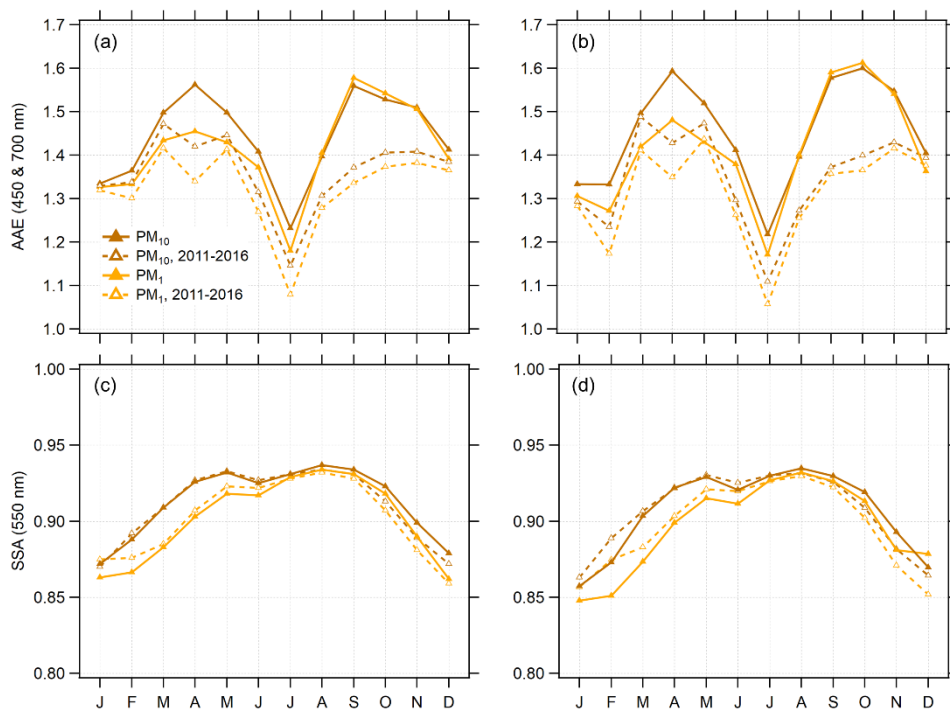
Figure S10: Monthly (a) median and (b) mean values of AAE (450 & 700 nm) and (c) median and (d) mean values of SSA (550 nm) at SPL. PM$_{10}$ data is represented with dark orange solid lines and PM$_1$ data is shown as light orange dashed lines. Values representing the entire SPL data range investigated in this work (2011-2024) are shown using closed markers, while values representing the data subrange of 2011-2016 are shown using open markers. Both medians and means are shown to make the data more comparable to that presented by Japngie-Green et al. (2019), wherein only monthly means were reported.
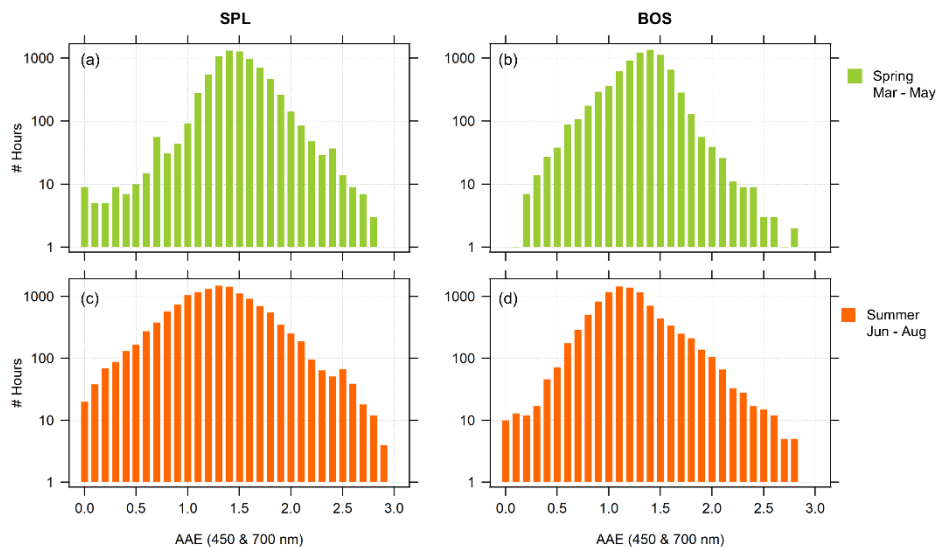
Figure S11: Histograms of hourly AAE data for the spring and summer periods at (**a, c**) SPL and (**b, d**) BOS. Note that the y-axis is a log scale.

150
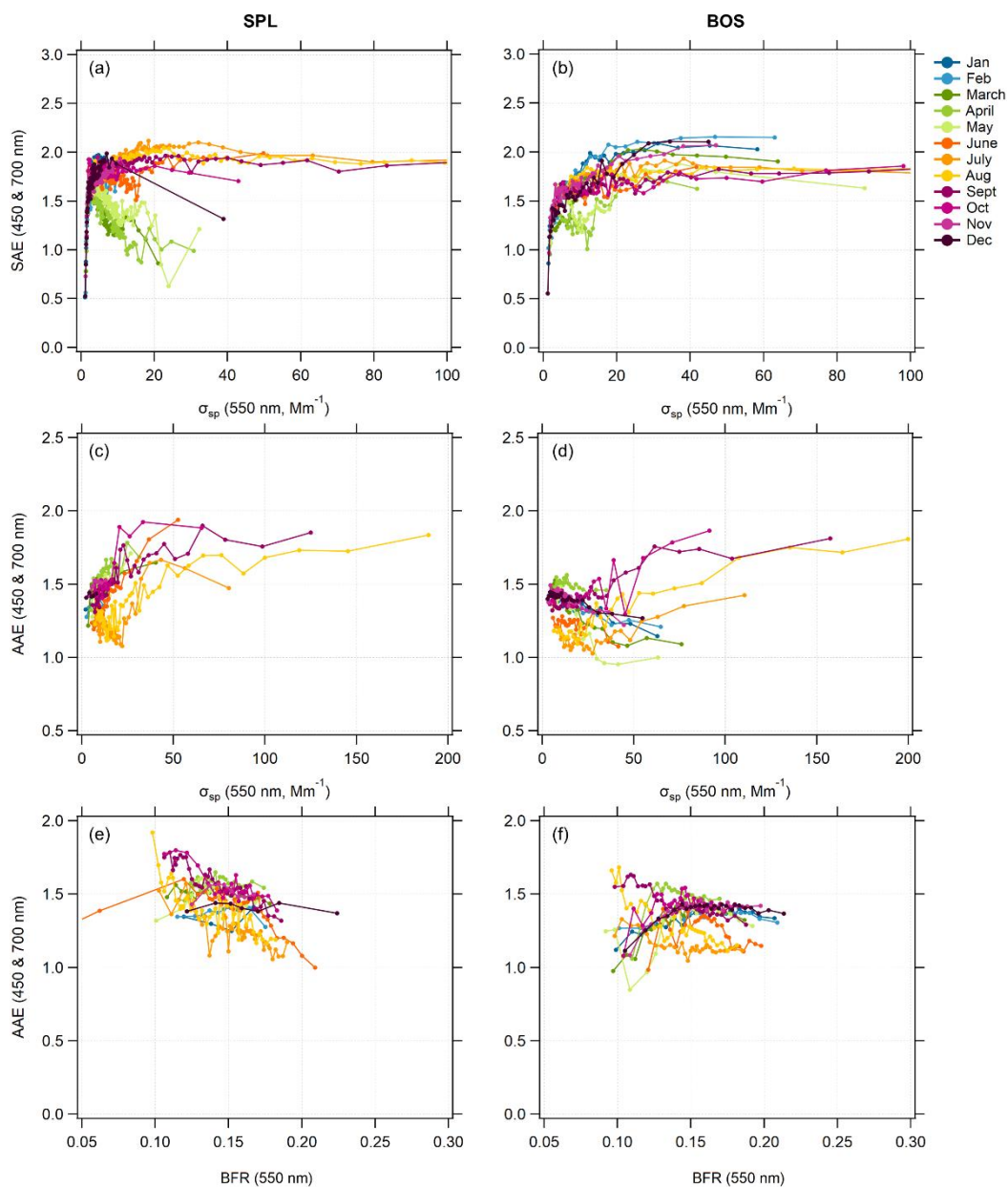
Figure S12: Top row is PM_{10} SAE (450 & 700 nm) binned by σ_{sp} (550 nm) for (a) SPL and (b) BOS. Middle row is PM_{10} AAE (450 & 700 nm) binned by the σ_{sp} (550 nm) for (c) SPL and (d) BOS. The bottom row is PM_{10} AAE (450 & 700 nm) binned by the Bfr (550 nm) for (e) SPL and (f) BOS. For all plots, each data point represents the median of 100 data points. Traces are colored by month according to the legend.

155
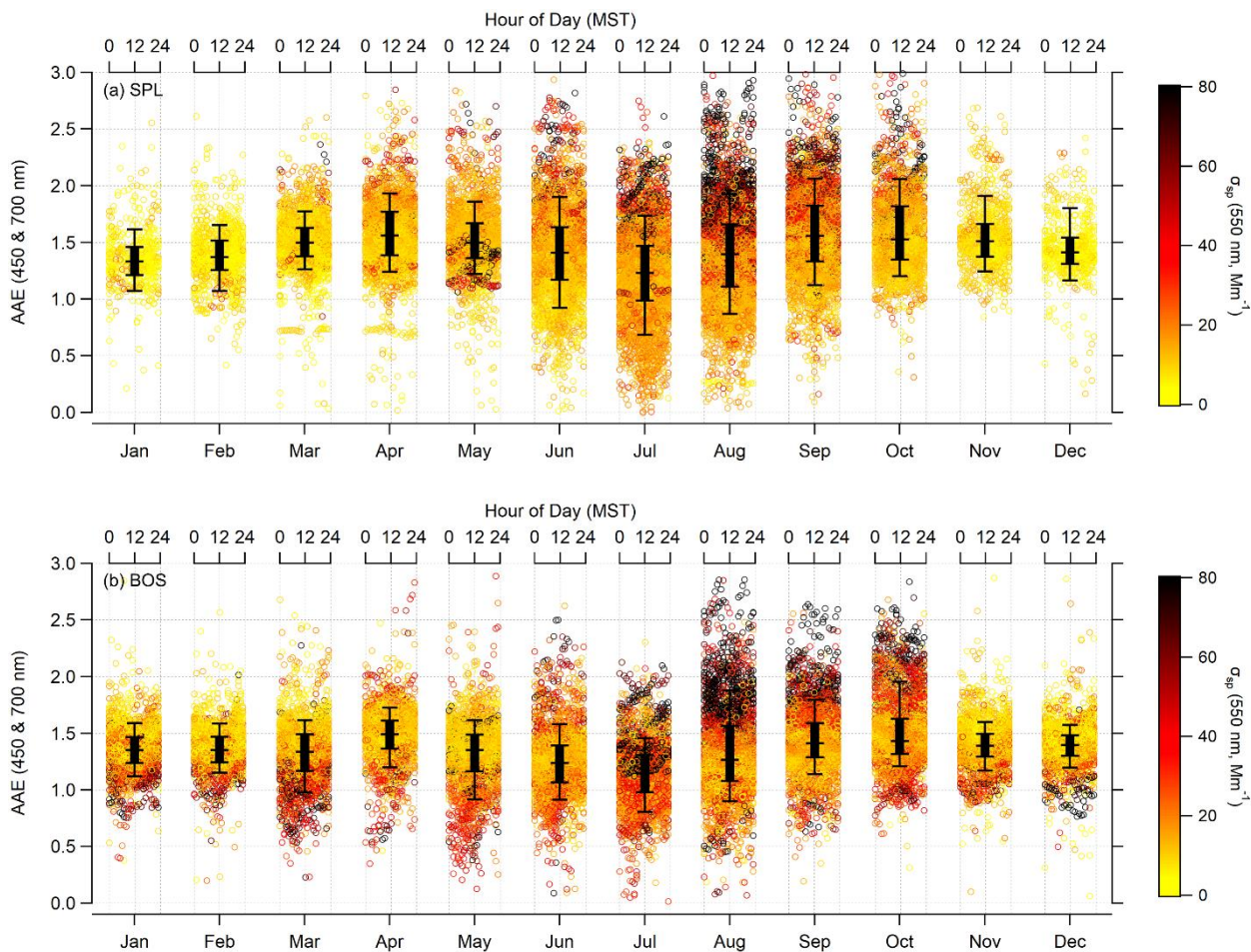
Figure S13: Monthly analysis of AAE values for (**a**) SPL and (**b**) BOS. For each plot the hourly AAE data for each month is shown, plotted by hour of day on the top axis and colored by the σ_{sp} (550 nm) value to show variation in AAE values with aerosol loadings. Monthly percentiles (10th, 25th, 50th, 75th, and 90th) for AAE are shown overtop the hourly data with black markers and bars.
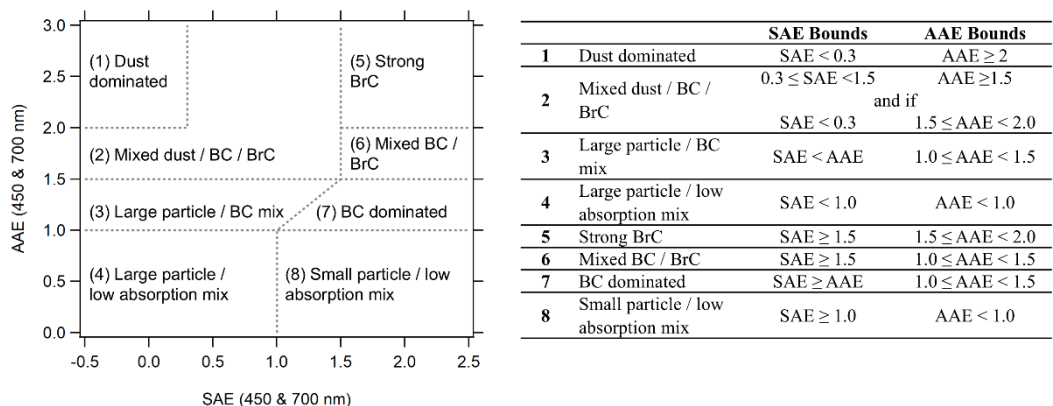
165

Figure S14: (left) Map of aerosol classification defined by Cappa et al. (2016). (right) Numeric bounds for each aerosol classification using the AAE and SAE values.
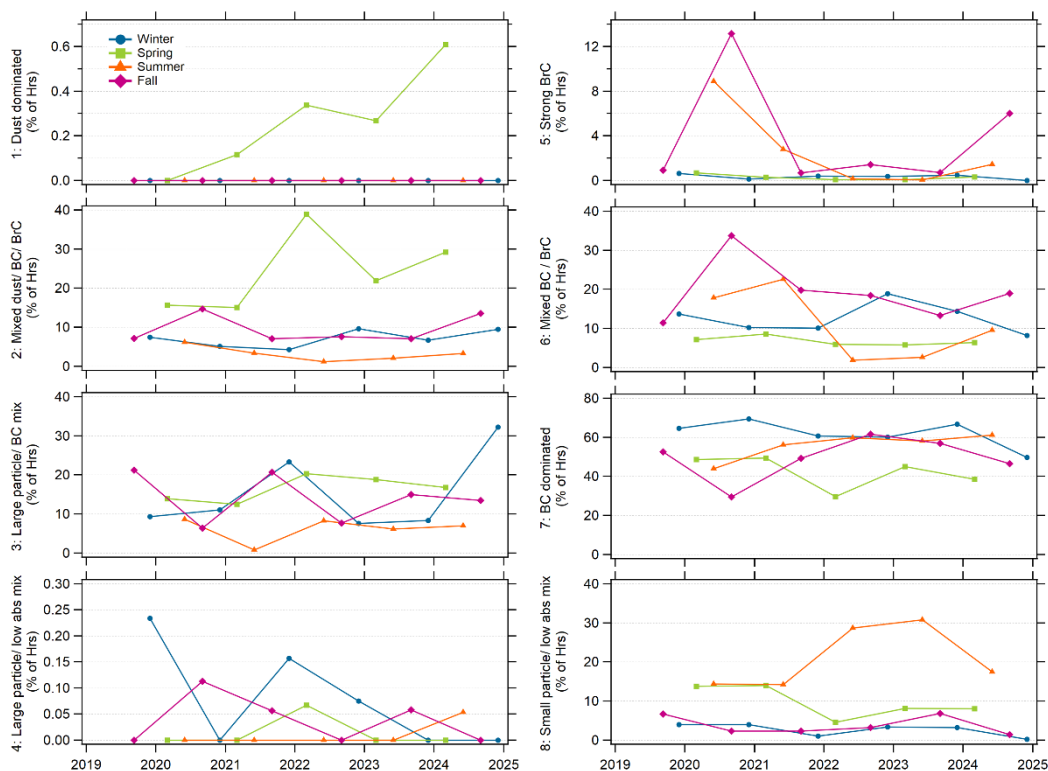
170 **Figure S15**: Percent of hours each season at BOS attributable to the 8 aerosol classifications defined by Cappa et al. (2016) over the entire measurement period. Note that the last winter data point at the end of the time series only represents data from December 2024.

175

Figure S16: Percent of hours each season at SPL attributable to the 8 aerosol classifications defined by Cappa et al. (2016) over the entire measurement period. Note that the last winter data point at the end of the time series only represents data from December 2024.

180
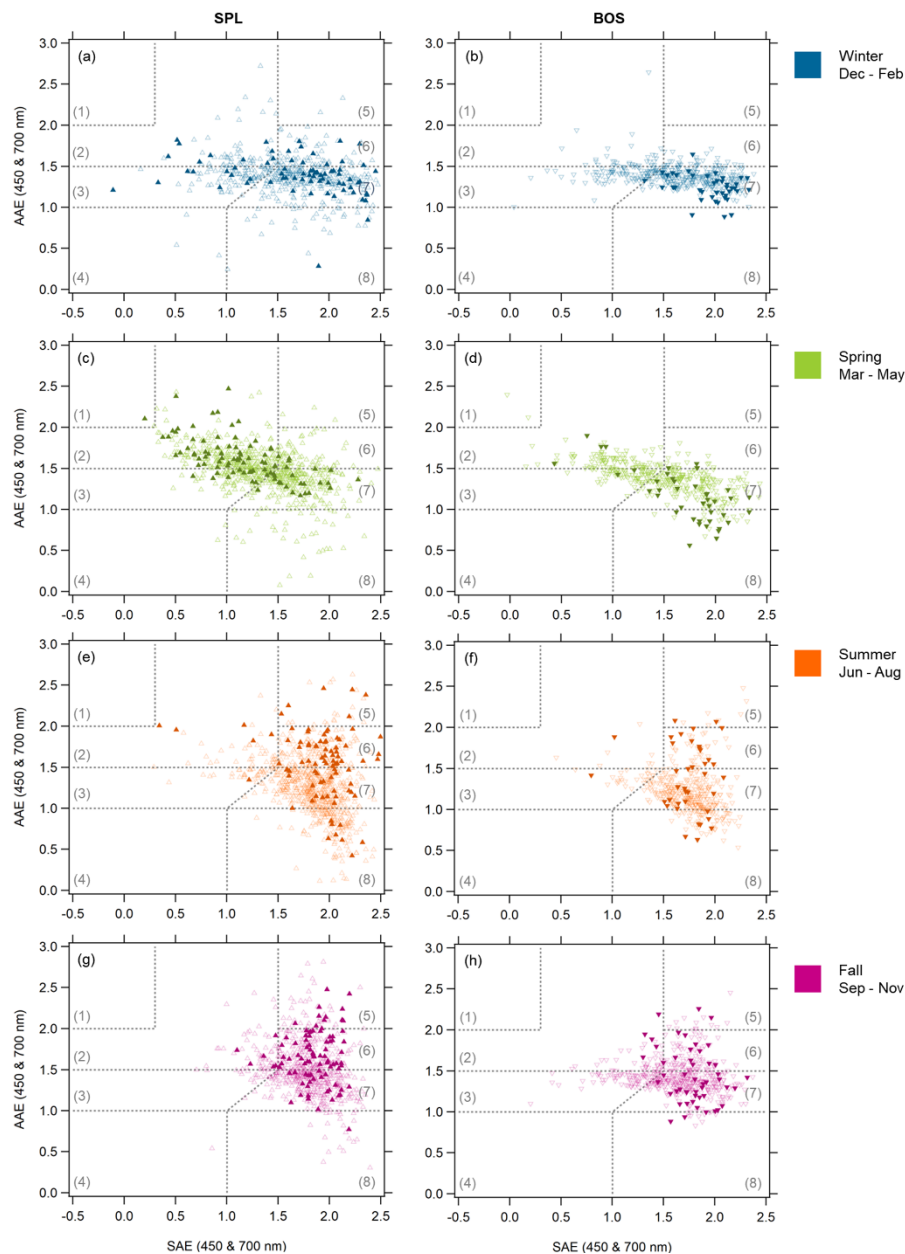
Figure S17: Daily medians of AAE vs SSA (450 & 700 nm) for all four seasons at (a, c, e, g) SPL and (b, d, f, h) BOS. Different regimes defined by Cappa et al. (2016) are outlined using grey markers and are labeled one through eight: (1) dust, (2) mixed dust/ BC/ BrC, (3) large particle / BC mix, (4) large particles with low absorption, (5) BrC, (6) mixed BC/ BrC, (7) BC, and (8) small particles with low absorption. For all data open markers show all data while closed markers show data where the daily average σ_{sp} value was above or equal to the 90th percentile for the month.

Table S7: Percent of hours per season in each of the eight aerosol regimes defined by Cappa et al. (2016). The average (μ) and standard deviation (σ) are reported in each cell as μ ± σ. Class descriptions can be found above in **Fig. S10**. Or each season, the aerosol classification representing the largest percentage of hours is shown in bold.

Class	SPL (2011 – 2024)				BOS (2019 – 2024)			
#	Winter	Spring	Summer	Fall	Winter	Spring	Summer	Fall
1	0.2 ± 0.4	1 ± 2	0.1 ± 0.1	0	0	0.3 ± 0.2	0	0
2	17 ± 16	**43 ± 18**	5 ± 3	6 ± 4	7 ± 2	20 ± 10	3 ± 2	10 ± 4
3	15 ± 6	19 ± 10	3 ± 3	2 ± 2	20 ± 10	16 ± 3	6 ± 3	14 ± 6
4	1 ± 1	0.1 ± 0.4	0	0.1 ± 0.1	0.1 ± 0.1	0.01 ± 0.03	0.01 ± 0.02	0.04 ± 0.05
5	2 ± 2	1 ± 1	4 ± 5	10 ± 9	0.3 ± 0. 2	0.3 ± 0.3	3 ± 4	4 ± 5
6	14 ± 9	8 ± 4	20 ± 10	34 ± 10	13 ± 4	7 ± 1	11 ± 9	19 ± 8
7	**45 ± 20**	26 ± 14	**47 ± 11**	**43 ± 19**	**62 ± 7**	**42 ± 8**	**56 ± 7**	**50 ± 10**
8	7 ± 9	3 ± 6	20 ± 10	4 ± 5	3 ± 2	10 ± 4	21 ± 8	4 ± 2

References

Bond, T. C., Anderson, T. L., and Campbell, D.: Calibration and Intercomparison of Filter-Based Measurements of Visible Light Absorption by Aerosols, Aerosol Sci. Technol, 30, 582–600, https://doi.org/10.1080/027868299304435, 1999.

Cappa, C. D., Kolesar, K. R., Zhang, X., Atkinson, D. B., Pekour, M. S., Zaveri, R. A., Zelenyuk, A., and Zhang, Q.: Understanding the optical properties of ambient sub- and supermicron particulate matter: results from the CARES 2010 field study in northern California, Atmos. Chem. Phys., 16, 6511–6535, https://doi.org/10.5194/acp-16-6511-2016, 2016.

Japngie-Green, C. M., Andrews, E., McCubbin, I. B., Ogren, J. A., and Hallar, A. G.: Climatology of Aerosol Optical Properties at Storm Peak Laboratory, Aerosol Air Qual. Res., 19, 1205–1213, https://doi.org/10.4209/aaqr.2018.05.0204, 2019.

Ogren, J. A.: Comment on "Calibration and Intercomparison of Filter-Based Measurements of Visible Light Absorption by Aerosols," Aerosol Sci. Technol, 44, 589–591, https://doi.org/10.1080/02786826.2010.482111, 2010.

Ogren, J. A., Wendell, J., Andrews, E., and Sheridan, P. J.: Continuous light absorption photometer for long-term studies, Atmos. Meas. Tech., 10, 4805–4818, https://doi.org/10.5194/amt-10-4805-2017, 2017.